

Dual-Polarized RSMA for Massive MIMO Systems

Arthur S. de Sena, *Student Member, IEEE*, Pedro H. J. Nardelli, *Senior Member, IEEE*, Daniel B. da Costa, *Senior Member, IEEE*, Petar Popovski, *Fellow, IEEE*, Constantinos B. Papadias, *Fellow, IEEE*, and Mérouane Debbah, *Fellow, IEEE*

Abstract—This work proposes a novel dual-polarized rate-splitting multiple access (RSMA) technique for massive multiple-input multiple-output (MIMO) networks. The proposed strategy transmits common and private symbols in parallel through dynamic polarization multiplexing, and it does not require successive interference cancellation (SIC) in the reception. For assisting the design of dual-polarized MIMO-RSMA systems, we propose a deep neural network (DNN) framework for predicting the ergodic sum-rates. An efficient DNN-aided adaptive power allocation policy is also developed for maximizing the ergodic sum-rates. Simulation results validate the effectiveness of the DNNs for sum-rate prediction and power allocation and reveal that the dual-polarized MIMO-RSMA strategy can impressively outperform conventional baseline schemes.

Index Terms—Dual-polarized MIMO, RSMA, deep learning.

I. INTRODUCTION

Rate-splitting multiple access (RSMA) has recently appeared as a powerful downlink transmission technique for multiple-input multiple-output (MIMO) systems. At the base station (BS), RSMA encodes the data messages of different users into common and private symbols and transmits them through linear precoding. Upon reception, users rely on successive interference cancellation (SIC) to recover the original message. The features of RSMA enable attractive performance improvements, such as higher data rates and robustness to imperfect channel state information (CSI). When RSMA is combined with massive MIMO systems, with a large number of antennas at the BS, further improvements can be achieved, outperforming conventional techniques like time-division multiple access (TDMA), space-division multiple access (SDMA), and non-orthogonal multiple access (NOMA) [1], [2].

Despite the advantages of RSMA, there are still unsolved issues and room for improvement. In particular, SIC introduces interference in the decoding process of RSMA, which is detrimental to the system spectral efficiency. Moreover, SIC error propagation can happen in practice, which also deteriorates the system performance. The recent work in [3] has shown that dual-polarized antenna arrays can be harnessed to alleviate SIC issues and improve user multiplexing. Moreover, dual-polarized antenna arrays are widely employed in commercial cellular systems and have been adopted as the standard in the 3rd generation partnership project (3GPP) long-term evolution advanced (LTE-A) and 5G New Radio (NR) specifications [3]. These facts imply that the polarization domain is a practical resource that is abundantly available and offers promising opportunities for enhancing the performance of next-generation communication systems. Under such

motivations, we propose an appealing dual-polarized RSMA strategy for dual-polarized massive MIMO systems, a concept not yet reported in the technical literature. With the goal of maximizing the system sum-rate, common and private symbols are multiplexed dynamically in the polarization domain. Our low-complexity strategy enables users to detect common and private symbols simultaneously from orthogonal polarizations without SIC, which reduces the overall interference experienced in the system. Due to the dynamic nature of the system model, classical performance analysis and optimization become unfeasible. Alternatively, we propose a deep neural network (DNN) framework for predicting the ergodic sum-rates of the proposed scheme. The DNN sum-rate prediction framework can be used as an efficient tool for assisting the design of dual-polarized MIMO-RSMA systems. To improve the ergodic sum-rate further, we also develop a DNN-aided adaptive power allocation framework, which smartly splits the transmit power between common and private symbols. Simulation results validate the effectiveness of the DNN frameworks and confirm that remarkable performance improvements are achievable with the dual-polarized MIMO-RSMA strategy.

Notation: The transpose and the Hermitian transpose of a matrix \mathbf{A} are represented by \mathbf{A}^T and \mathbf{A}^H , respectively. \mathbf{I}_M is the $M \times M$ identity matrix, $\mathbf{0}_{M,N}$ is the $M \times N$ matrix with all zero entries, and \otimes is the Kronecker product. Moreover, the cardinality of a set \mathcal{A} is represented by $|\mathcal{A}|$, \circ represents the function composition, and $\mathbb{E}[\cdot]$ denotes expectation.

II. SYSTEM MODEL

We consider a downlink single-cell scenario in which one base station (BS) employing $M/2$ co-located pairs of dual-polarized antennas (with vertical (v) and horizontal (h) polarizations) communicates with multiple users equipped with a single pair of dual-polarized antennas. The BS clusters the users into G groups, with each group containing N_g users. Users within a given group are assumed to share a common covariance matrix given by $\mathbf{R}_g = \mathbf{I}_2 \otimes \boldsymbol{\Sigma}_g = \mathbf{I}_2 \otimes (\mathbf{Q}_g \boldsymbol{\Delta}_g \mathbf{Q}_g^H)$, where $\boldsymbol{\Sigma}_g \in \mathbb{C}^{\frac{M}{2} \times \frac{M}{2}}$ denotes the covariance matrix of rank r_g observed in each polarization, $\boldsymbol{\Delta}_g$ is a real-valued $\bar{r}_g \times \bar{r}_g$ diagonal matrix containing $\bar{r}_g < r_g$ nonzero eigenvalues of $\boldsymbol{\Sigma}_g$, and \mathbf{Q}_g is a matrix comprising its corresponding eigenvectors. As a result, the dual-polarized channel matrix for the n th user in the g th group can be structured as

$$\mathbf{H}_{gn} = \begin{bmatrix} \mathbf{h}_{gv}^{vv} & \mathbf{h}_{gv}^{vh} \\ \mathbf{h}_{gv}^{hv} & \mathbf{h}_{gv}^{hh} \end{bmatrix} = \left[\mathbf{I}_2 \otimes \left(\mathbf{Q}_g \boldsymbol{\Delta}_g^{\frac{1}{2}} \right) \right] \begin{bmatrix} \mathbf{g}_{gn}^{vv} & \sqrt{\chi} \mathbf{g}_{gn}^{vh} \\ \sqrt{\chi} \mathbf{g}_{gn}^{hv} & \mathbf{g}_{gn}^{hh} \end{bmatrix}, \quad (1)$$

where $\mathbf{g}_{gn}^{ij} \in \mathbb{C}^{\bar{r}_g}$ denotes the reduced-dimension fast-fading channel vector from polarization i to j , with $i, j \in \{v, h\}$, and $\chi \in [0, 1]$ is the inverse cross-polar discrimination which measures the ratio of cross-polar to co-polar signal powers.

A. CSI Estimation and Acquisition

Due to quantization errors and other issues, the acquisition of \mathbf{g}_{gn}^{ij} at the BS is imperfect. As in [2], we model the

A. S. de Sena and Pedro H. J. Nardelli are with Lappeenranta-Lahti University of Technology, Finland, (email: arthur.sena@lut.fi, pedro.nardelli@lut.fi).

D. B. da Costa and Mérouane Debbah are with the Technology Innovation Institute (TII), Abu Dhabi, United Arab Emirates (e-mail: danielb-costa@ieee.org, merouane.debbah@tii.ae).

Petar Popovski is with Aalborg University, Denmark (e-mail: petarp@es.aau.dk).

C. B. Papadias is with The American College of Greece, Greece (e-mail: cpapadias@acg.edu).

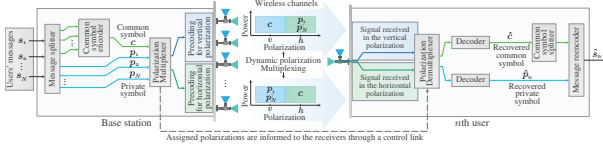


Fig. 1: Dual-polarized MIMO-RSMA transmitter. Private and common streams are transmitted in parallel via the polarization domain.

corrupted estimate of \mathbf{g}_{gn}^{ij} by

$$\hat{\mathbf{g}}_{gn}^{ij} = \sqrt{1 - \tau^2} \mathbf{g}_{gn}^{ij} + \tau \mathbf{z}_{gn}^{ij}, \quad (2)$$

where \mathbf{z}_{gn}^{ij} is a complex standard Gaussian random vector independent of \mathbf{g}_{gn}^{ij} , and τ is a factor that informs the quality of the CSI estimation, such that $\tau = 0$ corresponds to the perfect CSI case, and $\tau = 1$ models the extreme scenario where the estimate $\hat{\mathbf{g}}_{gn}^{ij}$ is statistically independent of \mathbf{g}_{gn}^{ij} .

On the other hand, we assume that Σ_g is perfectly known at the BS. In particular, the one-ring model [3] is adopted for generating Σ_g in this work.

B. Dual-Polarized Rate-Splitting Multiple Access

The proposed dual-polarized MIMO-RSMA strategy can be explained as follows. First, each user's message is split into a common and a private part. Then, the BS encodes the common parts into a single super-symbol, which we denote by x_g^c , and the private parts into private symbols, denoted by x_{gn}^p . The symbol x_g^c is intended for all users within the g th group, whereas x_{gn}^p should be decoded by the intended n th user only. In the original RSMA technique, x_g^c and x_{gn}^p are linearly precoded and superimposed in the power domain for transmission, which requires SIC in the reception. In contrast to conventional RSMA, our proposed technique transmits common and private symbols in parallel data streams via the polarization domain. More specifically, the BS transmits

$$\mathbf{x} = \sum_{g=1}^G \mathbf{P}_g \left(\sum_{n=1}^{N_g} \mathbf{w}_{gn}^p \sqrt{P \zeta_{gn} \alpha_{gn}^p} x_{gn}^p + \mathbf{w}_g^c \sqrt{P \zeta_{gn} \alpha_g^c} x_g^c \right), \quad (3)$$

where $\mathbf{P}_g \in \mathbb{C}^{M \times \bar{M}}$ is the precoding matrix for cancelling inter-group interference, in which \bar{M} determines the dimension of the transformed channel. The parameter P denotes the total transmit power, ζ_{gn} is the large-scale fading coefficient for the n th user in the g th group, and α_g^c and α_{gn}^p are the power allocation coefficients for the common and private symbols, with the constraint $\alpha_g^c + \sum_{n=1}^{N_g} \alpha_{gn}^p = 1$. In turn, $\mathbf{w}_g^c \in \mathbb{C}^{\bar{M}}$ and $\mathbf{w}_{gn}^p \in \mathbb{C}^{\bar{M}}$ are precoding vectors responsible for multiplexing the common and private symbols in polarizations i_g^c and i_g^p , respectively, such that $i_g^c \neq i_g^p \in \{v, h\}$, which are defined by

$$\mathbf{w}_g^c = \begin{bmatrix} \mathbf{w}_{g^c,v} \\ \mathbf{0} \end{bmatrix}, \quad \mathbf{w}_{gn}^p = \begin{bmatrix} \mathbf{0} \\ \mathbf{w}_{gn^p,h} \end{bmatrix}, \quad \text{if } i_g^c = v, \text{ and } i_g^p = h, \quad (4)$$

$$\mathbf{w}_g^c = \begin{bmatrix} \mathbf{0} \\ \mathbf{w}_{g^c,h} \end{bmatrix}, \quad \mathbf{w}_{gn}^p = \begin{bmatrix} \mathbf{w}_{gn^p,v} \\ \mathbf{0} \end{bmatrix}, \quad \text{if } i_g^c = h, \text{ and } i_g^p = v. \quad (5)$$

The polarizations i_g^c and i_g^p are assigned dynamically at each coherence interval by the BS. To this end, based on the estimated CSI modeled by (2), the BS predicts the instantaneous rates of the common and private symbols experienced by the users, denoted by \hat{R}_{gn}^c and \hat{R}_{gn}^p , and determines the desired polarizations based on the following criteria

$$\arg \max_{i_g^c, i_g^p} \sum_{n=1}^{N_g} \left[\hat{R}_{gn}^p + \min_{l \in \{1, \dots, N_g\}} \hat{R}_{gl}^c \right]. \quad (6)$$

After computing (6), the BS feeds back i_g^c and i_g^p to the users. In the reception, users within the g th group detects

the common message from polarization i_g^c and the private messages from polarization i_g^p . A simplified diagram of the proposed scheme is presented in Fig. 1.

C. Precoding for Inter-Group Interference Cancellation

After the signal in (3) has passed through the channel in (1), the n th user in the g th group receives:

$$\mathbf{y}_{gn} = \begin{bmatrix} \mathbf{g}_{gn}^{vv} & \sqrt{\chi} \mathbf{g}_{gn}^{vh} \\ \sqrt{\chi} \mathbf{g}_{gn}^{hv} & \mathbf{g}_{gn}^{hh} \end{bmatrix}^H \left[\mathbf{I}_2 \otimes \left(\Delta_{\frac{1}{2}} \mathbf{Q}_g^H \right) \right] \sum_{k=1}^G \mathbf{P}_k \times \left(\sum_{u=1}^{N_g} \mathbf{w}_{ku}^p \sqrt{P \zeta_{ku} \alpha_{ku}^p} x_{ku}^p + \mathbf{w}_k^c \sqrt{P \zeta_{ku} \alpha_k^c} x_k^c \right) + \begin{bmatrix} n_{gn}^v \\ n_{gn}^h \end{bmatrix}, \quad (7)$$

where n_{gn}^i denotes the additive noise observed by the n th user in polarization $i \in \{v, h\}$, which follows the complex Gaussian distribution with zero mean and variance σ^2 .

From (7), it is clear that the inter-group interference can be cancelled if, $\forall g \neq g'$, the following is satisfied

$$\left[\mathbf{I}_2 \otimes \left(\Delta_{\frac{1}{2}} \mathbf{Q}_{g'}^H \right) \right] \mathbf{P}_g = \left[\mathbf{I}_2 \otimes \left(\Delta_{\frac{1}{2}} \mathbf{Q}_{g'}^H \right) \right] (\mathbf{I}_2 \otimes \bar{\mathbf{P}}_g) = \mathbf{0}, \quad (8)$$

where $\bar{\mathbf{P}}_g \in \mathbb{C}^{\frac{M}{2} \times \bar{M}}$ is the precoding matrix for each polarization, in which $\bar{M} \triangleq M/2$. To this end, $\bar{\mathbf{P}}_g$ can be constructed by concatenating \bar{M} basis vectors of the null space of the matrix $\mathbf{Q} = [\mathbf{Q}_1, \dots, \mathbf{Q}_{g-1}, \mathbf{Q}_{g+1}, \dots, \mathbf{Q}_G] \in \mathbb{C}^{\frac{M}{2} \times \sum_{g'=1, g' \neq g}^G \bar{r}_{g'}}$, where $\bar{M} < M/2 - \sum_{g'=1, g' \neq g}^G \bar{r}_{g'}$. With this design, the signal in (7) can be simplified as

$$\mathbf{y}_{gn} = \begin{bmatrix} (\mathbf{g}_{gn}^{vv})^H \Delta_{\frac{1}{2}} \mathbf{Q}_g^H \bar{\mathbf{P}}_g & \sqrt{\chi} (\mathbf{g}_{gn}^{hv})^H \Delta_{\frac{1}{2}} \mathbf{Q}_g^H \bar{\mathbf{P}}_g \\ \sqrt{\chi} (\mathbf{g}_{gn}^{vh})^H \Delta_{\frac{1}{2}} \mathbf{Q}_g^H \bar{\mathbf{P}}_g & (\mathbf{g}_{gn}^{hh})^H \Delta_{\frac{1}{2}} \mathbf{Q}_g^H \bar{\mathbf{P}}_g \end{bmatrix} \times \left(\sum_{u=1}^{N_g} \mathbf{w}_{gu}^p \sqrt{P \zeta_{gu} \alpha_{gu}^p} x_{gu}^p + \mathbf{w}_g^c \sqrt{P \zeta_{gu} \alpha_g^c} x_g^c \right) + \begin{bmatrix} n_{gn}^v \\ n_{gn}^h \end{bmatrix}. \quad (9)$$

As a result, the n th user decodes the common message with following signal-to-interference-plus-noise ratio (SINR)

$$\gamma_{gn}^c = \frac{|(\mathbf{g}_{gn}^{ic})^H \Delta_{\frac{1}{2}} \mathbf{Q}_g^H \bar{\mathbf{P}}_g \mathbf{w}_g^{c,i_g^c}|^2 \rho \zeta_{gn} \alpha_g^c}{\chi \sum_{u=1}^{N_g} |(\mathbf{g}_{gn}^{i_g^c})^H \Delta_{\frac{1}{2}} \mathbf{Q}_g^H \bar{\mathbf{P}}_g \mathbf{w}_{gu}^{p,i_g^c}|^2 \rho \zeta_{gn} \alpha_{gu}^p + 1}, \quad (10)$$

where $\rho = P/\sigma^2$ denotes the signal-to-noise ratio (SNR), and the first term in the denominator models the cross-polar interference from polarization i_g^p to polarization i_g^c .

In turn, the SINR observed by the n th user in the g th group when decoding its private message can be represented by

$$\gamma_{gn}^p = \frac{|(\mathbf{g}_{gn}^{i_g^p})^H \Delta_{\frac{1}{2}} \mathbf{Q}_g^H \bar{\mathbf{P}}_g \mathbf{w}_{gn}^{p,i_g^p}|^2 \rho \zeta_{gn} \alpha_{gn}^p}{\chi |(\mathbf{g}_{gn}^{i_g^c})^H \Delta_{\frac{1}{2}} \mathbf{Q}_g^H \bar{\mathbf{P}}_g \mathbf{w}_g^{c,i_g^c}|^2 \rho \zeta_{gn} \alpha_g^c + \Psi_{gn}^{i_g^p} + 1}, \quad (11)$$

where the first term in the denominator corresponds to the cross-polar interference, and the term $\Psi_{gn}^{i_g^p} = \sum_{u=1, u \neq n}^{N_g} |(\mathbf{g}_{gn'}^{i_g^p})^H \Delta_{\frac{1}{2}} \mathbf{Q}_g^H \bar{\mathbf{P}}_g \mathbf{w}_{gu}^{p,i_g^p}|^2 \rho \zeta_{gn} \alpha_{gu}^p$ is the interference generated by imperfect CSI.

D. Precoding for the Common and Private Symbols

The precoding vector $\mathbf{w}_{gn}^{p,i_g^p} \in \mathbb{C}^{\bar{M}}$ should be designed to cancel the remaining inter-user interference observed in the assigned polarization $i_g^p \in \{v, h\}$ within each group. Mathematically, we must have $[(\mathbf{g}_{gn'}^{i_g^p})^H \Delta_{\frac{1}{2}} \mathbf{Q}_g^H \bar{\mathbf{P}}_g] \mathbf{w}_{gn}^{p,i_g^p} \approx 0$, for $\forall n' \neq n \in \{1, \dots, N_g\}$, i.e., the private precoder for one user must be near-orthogonal (orthogonal with perfect CSI) to the effective channels of other users. By defining $\hat{\mathbf{H}}_g^{i_g^p} = [\bar{\mathbf{P}}_g^H \mathbf{Q}_g \Delta_{\frac{1}{2}} \hat{\mathbf{g}}_{g1}^{i_g^p}, \dots, \bar{\mathbf{P}}_g^H \mathbf{Q}_g \Delta_{\frac{1}{2}} \hat{\mathbf{g}}_{gN_g}^{i_g^p}] \in \mathbb{C}^{\bar{M} \times N_g}$, the private precoder for the n th user can be computed as the zero-forcing precoder $\mathbf{w}_{gn}^{p,i_g^p} = [\hat{\mathbf{H}}_g^{i_g^p} ((\hat{\mathbf{H}}_g^{i_g^p})^H \hat{\mathbf{H}}_g^{i_g^p})^{-1}]_{:n}$, where $\bar{M} \geq N_g$ should be satisfied.

In turn, aiming at maximizing the worst observed SINR, \mathbf{w}_g^{c,i^c} can be obtained as follows:

$$\begin{aligned} \max_{\mathbf{w}_g^{c,i^c}} \quad & \min_{\forall l \in \{1, \dots, N_g\}} \gamma_{gn}^c, \\ \text{s.t.} \quad & \|\mathbf{w}_g^{c,i^c}\|^2 = 1. \end{aligned} \quad (12)$$

However, the problem in (12) is non-convex and NP-hard for general numbers of transmit antennas [4]. Fortunately, when $M \rightarrow \infty$, the asymptotic optimal \mathbf{w}_g^{c,i^c} is given by a linear combination of the effective channel vectors, as follows [5]

$$\mathbf{w}_g^{c,i^c} = \sum_{n=1}^{N_g} \mu_{gn} \bar{\mathbf{P}}_g^H \mathbf{Q}_g \Delta_g^{\frac{1}{2}} \hat{\mathbf{g}}_{gn}^{c,i^c}, \quad (13)$$

which consists of a weighted matched filter (MF) precoder for the channels of polarization $i^c \in \{v, h\}$, where μ_{gn} is the weight for the n th user in the g th group. As in [5], we employ an equally-weighted MF precoder, i.e., $\mu_{g1} = \dots = \mu_{gN_g} = \mu_g$. By defining $\boldsymbol{\omega}_g = \frac{1}{N_g} \sum_{n=1}^{N_g} \bar{\mathbf{P}}_g^H \mathbf{Q}_g \Delta_g^{\frac{1}{2}} \hat{\mathbf{g}}_{gn}^{c,i^c}$, μ_g is computed as $\mu_g^2 = 1/N_g^2 (\boldsymbol{\omega}_g^H \bar{\mathbf{P}}_g^H \bar{\mathbf{P}}_g \boldsymbol{\omega}_g)$, which satisfies the unity norm constraint in (12).

III. ERGODIC SUM-RATE ANALYSIS AND ADAPTIVE POWER ALLOCATION WITH DEEP NEURAL NETWORKS

A. Ergodic Sum-Rate

The instantaneous data rate for the n th user in the g th group is given by the sum of its private and common rates, which are calculated as $R_{gn}^p = \log_2(1 + \gamma_{gn}^p)$ and $R_{gn}^c = \min_{\forall l \in \{1, \dots, N_g\}} \{\log_2(1 + \gamma_{gl}^c)\}$, respectively. Thus, the ergodic sum-rate for the g th group can be obtained analytically through

$$\bar{R}_g = \sum_{n=1}^{N_g} \left(\int_0^\infty \log_2(1+x) f_{\gamma_{gn}^p}(x) dx + \int_0^\infty \log_2(1+y) f_{\gamma_{g(1)}^c}(y) dy \right), \quad (14)$$

where $f_{\gamma_{gn}^p}(x)$ is the probability density function (PDF) of γ_{gn}^p , and $f_{\gamma_{g(1)}^c}(y)$ denotes the PDF of the first order statistic of γ_{gn}^c , i.e., the PDF of $\min_{\forall l} \{\gamma_{gl}^c\}$. However, due to the correlated gains in the SINRs in (10) and (11), obtaining the exact expressions of $f_{\gamma_{gn}^p}(x)$ and $f_{\gamma_{g(1)}^c}(y)$ becomes a convoluted task. This complication makes the derivation of (14) intractable. Alternatively, we exploit the powerful capabilities of DNNs to approximate the desired sum-rate.

Given that the input parameters for \bar{R}_g form a compact subset, denoted by \mathcal{X}_g , and that \bar{R}_g is a real-valued continuous function, the universal approximation theorem [6, Theorem 2.2] ensures that a DNN with at least one hidden layer can approximate \bar{R}_g to any degree of accuracy, i.e.,

$$\sup_{\mathbf{x}_g \in \mathcal{X}_g} |\hat{R}_g - \bar{R}_g| < \epsilon, \quad (15)$$

for every $\epsilon > 0$, where \hat{R}_g is the function that models the DNN, and $\mathbf{x}_g \in \mathcal{X}_g \subseteq \mathbb{R}^{b_{\mathcal{X}_g}}$ represents the feature vector with $b_{\mathcal{X}_g}$ input parameters of the sum-rate function. This theorem provides theoretical support for the adoption of DNNs as predictors for the intricate multivariate expression in (14).

B. DNN for Ergodic Sum-Rate Prediction

We consider a DNN model with L dense layers, in which there are one input layer, one output layer, and $L - 2$ hidden layers, where the l th layer has Q_l neurons. For reducing the training complexity, we address the ergodic sum-rate for each spatial group separately. More specifically, the training dataset for users within the g th group is represented by $\mathcal{D}_g = \{(\mathbf{x}_{g,i}, \bar{R}_{g,i}) | \mathbf{x}_{g,i} \in \mathcal{X}_g, \bar{R}_{g,i} \in$

$\mathbb{R}, i = 1, \dots, |\mathcal{D}_g|\}$, where $\bar{R}_{g,i}$ is the target output, i.e., the actual ergodic sum-rate, of the i th training sample in \mathcal{D}_g , and $\mathbf{x}_{g,i}$ is the i th input sample vector containing $b_{\mathcal{X}_g} = 2N_g + 7$ system parameters, which are structured as $\mathbf{x}_{g,i} = [M, \bar{M}, N_g, \chi, \tau, \alpha_g^c, [\alpha_{g1}^p, \dots, \alpha_{gN_g}^p], [\zeta_{g1}, \dots, \zeta_{gN_g}], \rho]^T$. Note that the entries of $\mathbf{x}_{g,i}$ are within different ranges and that $\bar{R}_{g,i}$ can assume values from a broad interval, which can lead to an unstable and slow training convergence. To avoid this limitation, the training samples are scaled to the unity range. Under such considerations, ergodic sum-rate prediction function for the g th group can be expressed by

$$\hat{R}_g(\mathbf{x}_{g,i}) = \mathbf{r}_{L-1} \circ \mathbf{r}_{L-2} \circ \dots \circ \mathbf{r}_1(\mathbf{x}_{g,i}), \quad (16)$$

where $\mathbf{r}_l(\cdot)$ maps the transformation applied to the input data in the l th layer, which is defined by

$$\mathbf{r}_l(\mathbf{x}) = \pi_l(\mathbf{W}_l \mathbf{x} + \mathbf{b}_l), \forall l \in \{1, \dots, L-1\}, \quad (17)$$

in which \mathbf{x} is the input for the l th layer, $\mathbf{W}_l \in \mathbb{R}^{Q_l \times Q_{l-1}}$ is the weight matrix connecting the l th and $(l-1)$ th layers, and $\mathbf{b}_l \in \mathbb{R}^{Q_l}$ and $\pi_l: \mathbb{R}^{Q_l} \rightarrow \mathbb{R}^{Q_l}$ represent, respectively, the bias vector and activation function for the l th layer. In the hidden layers, we use as the activation function the rectified linear unity (ReLU), i.e., $\pi_l(\mathbf{x}) = \max(0, \mathbf{x})$, $\forall l \in \{1, \dots, L-2\}$, and in the output layer, a linear activation function is adopted.

For training, the data samples in \mathcal{D}_g are randomly selected and partitioned into J batches. As a result, the mean-squared error (MSE) loss function for the j th batch, $\forall j \in \{1, \dots, J\}$, to be minimized, can be written as

$$\mathcal{L}_{\mathcal{D}_{g,j}}(\boldsymbol{\Lambda}_g) = \frac{1}{S} \sum_{s=1}^S |\hat{R}_g(\mathbf{x}_{g,s}) - \bar{R}_{g,s}|^2, \quad (18)$$

where $\mathcal{D}_{g,j} = \{(\mathbf{x}_{g,s}, \bar{R}_{g,s}) | s = 1, \dots, S\} \subseteq \mathcal{D}_g$ represents the subset corresponding to the j th data batch, in which S denotes the cardinality of $\mathcal{D}_{g,j}$, i.e., the batch size.

C. DNN-Aided Adaptive Power Allocation

Following the work in [5], the power allocation adopted for the private symbols is computed by $\alpha_{gu}^p = (1 - \alpha_g^c)/N_g$, which consists of a uniform allocation policy given as a function of the power coefficient for the common symbol. Therefore, the challenge with this strategy remains in determining the coefficient α_g^c . In particular, our goal is to maximize the ergodic sum-rate, which can be formulated as

$$\begin{aligned} \arg \max_{\alpha_g^c} \quad & \sum_{n=1}^{N_g} \mathbb{E} \left[\log_2(1 + \gamma_{gn}^p) + \min_{\forall l} \{\log_2(1 + \gamma_{gl}^c)\} \right], \\ \text{s.t.} \quad & \alpha_g^c \leq 1. \end{aligned} \quad (19)$$

However, due to the dynamic polarization multiplexing, the coupled SNRs in (10) and (11), and the coupled coefficients α_g^c and α_{gu}^p , a closed-form optimal solution for (19) cannot be obtained. Determining the desired coefficient through an exhaustive search is also a possibility. However, brute-force strategies can be computationally expensive, which is not ideal for real-time communication. On the other hand, DNNs offer a short run-time after trained. With this motivation, we propose a DNN framework for approximating the optimal power coefficient. To this end, for each spatial group, we train a DNN model with one input layer, one output layer, and $D-2$ hidden layers, with the d th layer having V_d neurons.

Specifically, for training the DNN for power allocation, we use the dataset $\mathcal{M}_g = \{(\mathbf{z}_{g,i}, \alpha_{g,i}^{c*}) | \mathbf{z}_{g,i} \in \mathcal{Z}_g, \alpha_{g,i}^{c*} \in$

$\mathbb{R}, i = 1, \dots, |\mathcal{M}_g|$, where $\alpha_{g,i}^{c*}$ is the target power coefficient that maximizes the ergodic sum-rate for the i th input vector $\mathbf{z}_{g,i} \in \mathcal{Z}_g \subseteq \mathbb{R}^{b_{\mathcal{Z}_g}}$, which is defined by $\mathbf{z}_{g,i} = [M, \bar{M}, N_g, \chi, \tau, [\zeta_{g1}, \dots, \zeta_{gN_g}], \rho]^T$. Both $\mathbf{z}_{g,i}$ and $\alpha_{g,i}^{c*}$ are achieved by exploiting the existing datasets \mathcal{D}_g . That is, for each sample $\mathbf{z}_{g,i}$, we select the power coefficient that maximizes the corresponding sum-rate in \mathcal{D}_g and create the new dataset \mathcal{M}_g . As in subsection III-B, the vectors $\mathbf{z}_{g,i}$ are scaled to the unity range. As a result, the function that predicts the optimal power allocation coefficient can be written as

$$\hat{\Lambda}_g(\mathbf{z}_{g,i}) = \mathbf{r}_{D-1} \circ \mathbf{r}_{D-2} \circ \dots \circ \mathbf{r}_1(\mathbf{z}_{g,i}), \quad (20)$$

where $\mathbf{r}_d(\cdot)$ is defined as in (17), in which ReLU activation functions are employed in the hidden layers and a linear function in the output layer. We also adopt the MSE loss function in this model. Moreover, for satisfying the constraint in (19), the power coefficient is computed by $\hat{\alpha}_g^{c*} = \min\{1, \hat{\Lambda}_g(\mathbf{z}_{g,i})\}$.

D. Complexity Remarks

Note that we implement one DNN model for each spatial group. The main implication of this choice is that the covariance matrices, which have large dimensions, are not required for designing and training the DNNs. Consequently, we can considerably simplify the model architecture and decrease the training complexity. In practice, DNNs can be trained very efficiently in specialized hardware. Therefore, the complexity of the testing phase is more relevant for the practical operation of the proposed scheme. Specifically, the computational complexity of one forward pass can be expressed in terms of floating-point operations [7]. Under this analysis, the DNN for sum-rate prediction has a complexity of $\mathcal{O}(\sum_{l=1}^L Q_{l-1}Q_l)$. For the DNN-aided power allocation strategy, on the other hand, it is also important to mention the complexity associated with the generation of the dataset with optimal power coefficients. More specifically, we need to perform an exhaustive search on the dataset \mathcal{D}_g to construct \mathcal{M}_g , which imposes additional complexity. Nevertheless, this search needs to be executed only once before the training, thus, it is a computationally affordable task. After the dataset \mathcal{M}_g is properly generated and the DNN is trained, the desired power coefficient is computed with a complexity of $\mathcal{O}(\sum_{d=1}^D V_{d-1}V_d)$ in the testing phase¹.

E. Datasets Generation and DNN Implementation

Due to the unknown PDFs of γ_{gn}^p and $\min_{\forall l}\{\gamma_{gl}^c\}$, we cannot generate the datasets \mathcal{D}_g and \mathcal{M}_g , $g \in \{1, \dots, G\}$, with the expression in (14). Due to this reason, instead, we used Monte Carlo simulations for obtaining the required data samples, in which the high-performance Julia Programming Language [8] has been used for implementing the proposed MIMO-RSMA network. For generating the training data, we adjusted the number of groups to $G = 3$, and the number of users within each group to $N_1 = \dots = N_g = 3$. Consequently, the resulting number of features in the i th input vectors $\mathbf{x}_{g,i}$ and $\mathbf{z}_{g,i}$ were $b_{\mathcal{X}_g} = 13$ and $b_{\mathcal{Z}_g} = 9$, respectively. Then, we have extensively varied the system parameters and generated for each group a total of 6,561,000 samples for \mathcal{D}_g , and

¹The complexity trade-offs between the proposed dual-polarized MIMO-RSMA with the DNN-aided power allocation and the conventional MIMO-RSMA still need to be better investigated, which arises as a potential future research direction.

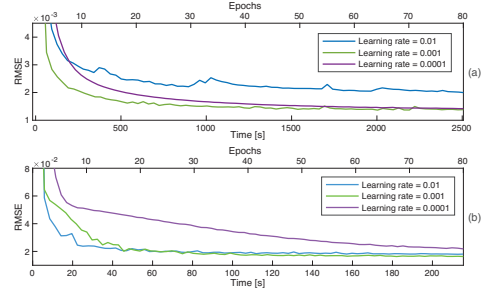


Fig. 2: Training convergence behavior in terms of RMSE for: (a) DNN for ergodic sum-rate prediction, and (b) DNN for adaptive power allocation.

72,900 samples for \mathcal{M}_g , where each sample was generated by averaging 2×10^3 random channel realizations. Moreover, 90% of the samples were used for training and 10% for testing.

The DNN models were implemented and trained in Python 3.9.11 using Tensor Flow Metal 2.8.0. The DNN for sum-rate prediction was implemented with five hidden layers, with the first and last hidden layers comprising 128 neurons and the remaining layers comprising 256 neurons each. In turn, the DNN for power allocation was implemented with four hidden layers, with the first and last hidden layers also containing 128 neurons and the remaining layers containing 256 neurons. For training the DNNs, we adopted the adaptive moment estimation (ADAM) optimizer. Moreover, the batch sizes for sum-rate prediction and power allocation were adjusted to 1000 and 100 samples, respectively, and both DNNs were trained for 80 epochs. Fig. 2 presents the training convergence in terms of root mean squared error (RMSE) for the two DNNs. As can be seen, the learning rate of 0.001 achieves the lowest RMSE. Thus, this value is adopted in the next section.

IV. SIMULATION RESULTS

The DNNs for sum-rate prediction and power allocation are evaluated in this section. The performance superiority of the proposed dual-polarized MIMO-RSMA scheme is also demonstrated over conventional baseline systems, including the single-polarized MIMO-RSMA, MIMO-TDMA, MIMO-SDMA, MIMO-NOMA, and the dual-polarized MIMO-NOMA approach proposed in [9]. In all systems, we configure the BS with $M = 64$ transmit antennas, and we consider that users are distributed within $G = 3$ spatial groups. Without loss of generality, we present results for the first group, which contains $N = 3$ users, is located at the azimuth angle of 20° , and has an angular spread of 11° . Moreover, the distances from the BS to users 1, 2, and 3 are set to $d_1 = 115$ m, $d_2 = 100$ m, and $d_3 = 85$ m, respectively. Under this setting, the large-scale fading coefficient for each user is modeled by $\zeta_n = \delta d_n^{-\eta}$, where δ is an array gain parameter adjusted to 40 dB, and η is the path-loss exponent set to 2.7. Furthermore, we set $\bar{M} = 6$ and adjust the total transmit power to $P = 1$ W. Unless otherwise stated, when fixed power allocation is employed, we set $\alpha^c = 0.5$ and $\alpha_n^p = (1 - \alpha^c)/N \approx 0.17$ for the MIMO-RSMA schemes, whereas, for the MIMO-NOMA counterpart, we set the coefficients of users 1, 2, and 3 to $5/8, 2/8$, and $1/8$, respectively. In turn, a uniform power allocation is employed in the MIMO-SDMA systems, and in the MIMO-TDMA, the full transmit power, P , is used at each time slot.

Fig. 3 validates the DNN framework for ergodic sum-rate prediction under fixed power allocation. As can be seen, the

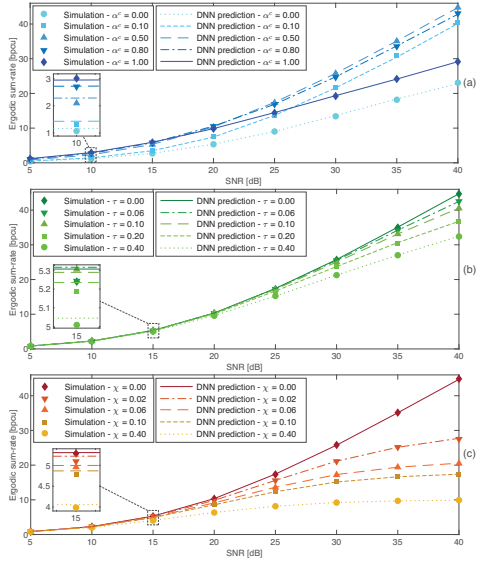


Fig. 3: Simulated and predicted ergodic sum-rates: (a) for different values of α^c , with $\chi = 0$ and $\tau = 0$, (b) for different values of τ , with $\alpha^c = 0.5$ and $\chi = 0$, and (c) for different values of χ , with $\alpha^c = 0.5$ and $\tau = 0$.

predicted curves can follow the simulated ones with high accuracy in all considered cases. This figure also provides the first insights into the performance behavior of the proposed dual-polarized MIMO-RSMA scheme. Fig. 3(a), for instance, shows that the power coefficient for the common message plays an important role in the ergodic sum-rate performance and that the optimal power coefficient changes with the observed SNR. Fig. 3(b) reveals how imperfect CSI impacts the sum-rate of the proposed strategy. As can be seen, even though the system performance deteriorates with the increase of τ , a remarkable sum-rate of more than 30 bits per channel use (bps/c) can be achieved even when $\tau = 0.4$, which confirms robustness to imperfect CSI. On the other hand, as can be seen in Fig. 3(c), the dual-polarized MIMO-RSMA is more severely impacted by polarization interference (with fixed power allocation).

The ergodic sum-rates achieved with the dual-polarized MIMO-RSMA scheme and with the conventional systems are compared in Fig. 4. As we can see in Fig. 4(a), when $\chi = 0$, the dual-polarized MIMO-RSMA systems always achieve the best performance. However, with $\chi = 0.2$, the dual-polarized MIMO-RSMA scheme with fixed power allocation becomes less spectrally efficient than the single-polarized MIMO-RSMA and MIMO-SDMA counterparts. In contrast, by smartly splitting the transmit power between private and common streams, the proposed dual-polarized approach with the DNN-aided power allocation can impressively outperform all conventional baseline schemes despite the high interference. The effectiveness of our proposal is further corroborated in Fig. 4(b), where we plot the ergodic sum-rates versus the CSI quality factor τ . As can be seen, the dual-polarized MIMO-RSMA scheme with the DNN power allocation achieves the highest sum-rates for all values of τ and χ . The reason for such robustness is that the DNN mitigates the effects of both imperfect CSI and cross-polar interference by smartly adjusting α_g^c . For instance, the DNN assigns power only to one polarization if χ becomes excessively high for tackling cross-polar interference or allocates more power to the common stream when the CSI becomes degraded. Last, Fig.

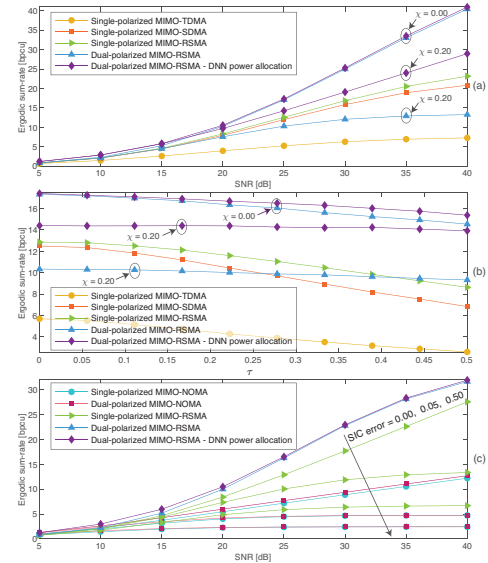


Fig. 4: Simulated ergodic sum-rates: (a) versus SNR for different levels of χ , with $\tau = 0.1$, (b) versus τ for a SNR of 25 dB and different levels of χ , and (c) versus SNR for different levels of SIC error, with $\chi = 0.01$ and $\tau = 0$. 4(c) compares the sum-rate performance of the dual-polarized MIMO-RSMA and of SIC-based schemes under the effects of SIC error propagation. The sum-rates of the schemes that rely on SIC are strongly degraded when the SIC error factor increases. On the other hand, the robust dual-polarized MIMO-RSMA is unaffected by SIC issues.

V. CONCLUSIONS

We have proposed a novel low-complexity dual-polarized massive MIMO-RSMA scheme, which is free from the interference issues of SIC and robust to imperfect CSI. We have also developed DNN frameworks for ergodic sum-rate prediction and efficient power allocation, which ensured high performance even under strong cross-polar interference.

REFERENCES

- [1] B. Clerckx, Y. Mao, R. Schober, E. A. Jorswieck, D. J. Love, J. Yuan, L. Hanzo, G. Y. Li, E. G. Larsson, and G. Caire, "Is NOMA efficient in multi-antenna networks? A critical look at next generation multiple access techniques," *IEEE Open J. Commun. Soc.*, vol. 2, pp. 1310–1343, 2021.
- [2] O. Dizdar, Y. Mao, and B. Clerckx, "Rate-splitting multiple access to mitigate the curse of mobility in (massive) mimo networks," *IEEE Trans. Commun.*, vol. 69, no. 10, pp. 6765–6780, 2021.
- [3] A. S. de Sena, P. H. J. Nardelli, D. B. da Costa, F. R. M. Lima, L. Yang, P. Popovski, Z. Ding, and C. B. Papadias, "IRS-assisted massive MIMO-NOMA networks: Exploiting wave polarization," *IEEE Trans. Wireless Commun.*, vol. 20, no. 11, pp. 7166–7183, 2021.
- [4] Z. Xiang, M. Tao, and X. Wang, "Massive MIMO multicasting in noncooperative cellular networks," *IEEE J. Sel. Areas Commun.*, vol. 32, no. 6, pp. 1180–1193, 2014.
- [5] M. Dai, B. Clerckx, D. Gesbert, and G. Caire, "A rate splitting strategy for massive MIMO with imperfect CSIT," *IEEE Trans. Wireless Commun.*, vol. 15, no. 7, pp. 4611–4624, 2016.
- [6] K. Hornik, M. Stinchcombe, and H. White, "Multilayer feedforward networks are universal approximators," *Neural Netw.*, vol. 2, no. 5, pp. 359–366, Jan. 1989.
- [7] Y. Yang, F. Gao, Z. Zhong, B. Ai, and A. Alkhatieb, "Deep transfer learning-based downlink channel prediction for FDD massive MIMO systems," *IEEE Trans. Commun.*, vol. 68, no. 12, pp. 7485–7497, 2020.
- [8] J. Bezanson, A. Edelman, S. Karpinski, and V. B. Shah, "Julia: A fresh approach to numerical computing," *SIAM Review*, vol. 59, no. 1, pp. 65–98, 2017.
- [9] A. S. de Sena, D. B. da Costa, Z. Ding, and P. H. J. Nardelli, "Massive MIMO-NOMA networks with multi-polarized antennas," *IEEE Trans. Wireless Commun.*, vol. 18, no. 12, pp. 5630–5642, Dec. 2019.